arXiv:2002.04398v1 [quant-ph] 4 Feb 2020

$\mathcal{PT}$-symmetric potentials having continuous spectra

Zichao Wen* **and Carl M Bender†**

*Department of Obstetrics and Gynecology, Washington University School of Medicine, St. Louis, Missouri 63110, USA
email: zwen@wustl.edu
†Department of Physics, Washington University, St. Louis, MO 63130, USA
email: cmb@wustl.edu

Abstract. One-dimensional $\mathcal{PT}$-symmetric quantum-mechanical Hamiltonians having continuous spectra are studied. The Hamiltonians considered have the form $H = p^2 + V(x)$, where $V(x)$ is odd in x, pure imaginary, and vanishes as $|x| \to \infty$. Five $\mathcal{PT}$-symmetric potentials are studied: the Scarf-II potential $V_1(x) = iA_1\,\mathrm{sech}(x)\tanh(x)$, which decays exponentially for large $|x|$; the rational potentials $V_2(x) = iA_2\,x/(1+x^4)$ and $V_3(x) = iA_3\,x/(1+|x|^3)$, which decay algebraically for large $|x|$; the step-function potential $V_4(x) = iA_4\,\mathrm{sgn}(x)\theta(2.5-|x|)$, which has compact support; the regulated Coulomb potential $V_5(x) = iA_5\,x/(1+x^2)$, which decays slowly as $|x| \to \infty$ and may be viewed as a long-range potential. The real parameters A_n measure the strengths of these potentials. Numerical techniques for solving the time-independent Schrödinger eigenvalue problems associated with these potentials reveal that the spectra of the corresponding Hamiltonians exhibit universal properties. In general, the eigenvalues are partly real and partly complex. The real eigenvalues form the continuous part of the spectrum and the complex eigenvalues form the discrete part of the spectrum. The real eigenvalues range continuously in value from 0 to $+\infty$. The complex eigenvalues occur in discrete complex-conjugate pairs and for $V_n(x)$ $(1 \le n \le 4)$ the number of these pairs is finite and increases as the value of the strength parameter A_n increases. However, for $V_5(x)$ there is an *infinite* sequence of discrete eigenvalues with a limit point at the origin. This sequence is complex, but it is similar to the Balmer series for the hydrogen atom because it has inverse-square convergence.

Submitted to: *J. Phys. A: Math. Gen.*

1. Introduction

A $\mathcal{PT}$-symmetric quantum theory is defined by a Hamiltonian that is invariant under combined space reflection (parity) $\mathcal{P}$ and time reversal $\mathcal{T}$. An early class of non-Hermitian $\mathcal{PT}$-symmetric Hamiltonians that has been studied in depth is $H = p^2 + x^2(ix)^\varepsilon$ (ε real). These Hamiltonians are $\mathcal{PT}$ invariant because $x \to -x$ under $\mathcal{P}$ and $i \to -i$ under $\mathcal{T}$. It was observed in Refs. [1, 2] that the eigenvalues of this class of Hamiltonians are real, discrete, and positive for all $\varepsilon \ge 0$ and the reality of these eigenvalues was attributed to the $\mathcal{PT}$ symmetry of H. Subsequently, the reality of the spectrum was established at a mathematically rigorous level in Refs. [3, 4].

The eigenvalues of a $\mathcal{PT}$-symmetric Hamiltonian are either real or come in complex-conjugate pairs. If the eigenvalue spectrum is entirely real, the $\mathcal{PT}$ symmetry of the Hamiltonian is said to be *unbroken*, but if some of the eigenvalues are complex, the $\mathcal{PT}$ symmetry of the Hamiltonian is said to be *broken*. Many studies of model quantum systems whose Hamiltonians are $\mathcal{PT}$ invariant have been published (see Refs. [5, 11]). $\mathcal{PT}$-symmetric Hamiltonians often exhibit a transition from a parametric region of unbroken $\mathcal{PT}$ symmetry to a region of broken $\mathcal{PT}$ symmetry. This $\mathcal{PT}$ transition occurs in both the classical and in the quantized versions of a $\mathcal{PT}$-symmetric Hamiltonian [2] and this transition has been observed in numerous laboratory experiments [5, 11].

Many papers on $\mathcal{PT}$-symmetric Hamiltonians having discrete spectra have been published, but there have been only very few studies of $\mathcal{PT}$-symmetric Hamiltonians having continuous spectra. Therefore, in this paper we consider Hamiltonians $H = p^2 + V(x)$ whose potentials possess continuous spectra. The potentials $V(x)$ that we discuss here decay to 0 as $|x| \to \infty$. Thus, it is not surprising that we find that in general the real part of the spectrum is continuous and that these eigenvalues range continuously from 0 to $+\infty$. Since the potential $V(x)$ is *odd* under $x \to -x$ and is pure imaginary, $V(x)$ is $\mathcal{PT}$ invariant, and hence complex eigenvalues must appear as complex-conjugate pairs. On the basis of our study we believe that short-range potentials typically have a finite number of discrete complex eigenvalues and that long-range potentials have an infinite number of discrete complex eigenvalues.

To be specific, in this paper we study five one-dimensional Hamiltonians of the form $H_n = p^2 + V_n(x)$, where

$$\begin{aligned} V_1(x) &= iA_1\,\mathrm{sech}(x)\tanh(x), \\ V_2(x) &= iA_2\,x/(1+x^4), \\ V_3(x) &= iA_3\,x/(1+|x|^3), \\ V_4(x) &= iA_4\,\mathrm{sgn}(x)\theta(2.5-|x|), \\ V_5(x) &= iA_5\,x/(1+x^2), \end{aligned} \tag{1}$$

and the strength parameters A_n are real. In all cases $V_n(x)$ is odd in x and is pure imaginary, so the H_n are all $\mathcal{PT}$ symmetric. Furthermore, these potentials all vanish as $|x| \to \infty$. In all these cases the Hamiltonians H_n have real eigenvalues that range continuously from 0 to $+\infty$. However, the universal property of the five Hamiltonians studied here is that in addition to the real continuous part of the spectra, there are complex-conjugate pairs of discrete eigenvalues for sufficiently large strength parameters A_n. Thus, in all these cases the $\mathcal{PT}$ symmetry of these Hamiltonians H_n is broken.

The five potentials $V_n(x)$ vanish at different rates for large $|x|$: The Scarf-II potential $V_1(x)$ decays exponentially for large $|x|$ [6, 7, 8, 9], the rational potentials $V_2(x)$ and $V_3(x)$ decay algebraically like $|x|^{-3}$ and $|x|^{-2}$ for large $|x|$, and the step-function potential $V_4(x)$ has compact support [10]. These are all *short-range* potentials and we find that these potentials confine a *finite* number of discrete complex bound states. The number and size of these complex eigenvalues increase as the strength parameters A_n increase.

The potential $V_5(x)$ is special; it vanishes slowly like $1/|x|$ for large $|x|$. Because

it vanishes slowly,/and to it is a *long-range* potential like the Coulomb potential. Even though this potential is bounded, the property that it is long range allows it to confine *infinitely many* discrete complex bound states. Like the Balmer series for the hydrogen atom, the sequence of complex-conjugate pairs of eigenvalues converges to a limit point, which happens to be at 0, and the kth pair of eigenvalues approaches 0 like $1/k^2$.

In previous studies of $\mathcal{PT}$-symmetric Hamiltonians it was found that accurate numerical calculations of real discrete eigenvalues could be done by using the shooting method [1]. However, if the discrete eigenvalues are complex, the shooting method becomes unwieldy. Therefore, alternative techniques based on the finite-element and variational methods were used. A numerical technique known as the *Arnoldi algorithm* was used in Ref. [12].

Let us summarize the numerical technique used in this paper: For numerical calculations of eigenvalues one cannot work directly on the infinite x axis, so one reduces the problem to solving the Schrödinger equation on a large but *finite* interval. Consequently, the numerical techniques used to calculate eigenvalues can only return discrete values and one must determine whether a given eigenvalue belongs to a discrete or a continuous part of the spectrum. To distinguish between these two possibilities we examine the associated eigenfunctions and observe how they satisfy the boundary conditions. As explained in detail in Ref. [12], the eigenfunctions associated with discrete eigenvalues are localized in space (like bound states) and decay to 0 smoothly and exponentially as x approaches the boundary points of the interval. However, the eigenfunctions for eigenvalues that belong to the continuous part of the spectrum drop abruptly to 0 at one or both endpoints of the finite interval.

The technique used here to compute the eigenvalues of H_n is called *Chebyshev spectral collocation*. This technique relies on the properties of Chebyshev polynomials and Chebyshev series and is explained in detail in Ref. [13]. To calculate the spectra of the Hamiltonians H_n by using Chebyshev spectral collocation we replace the infinite x axis by the finite interval $-L \le x \le L$. We then decompose the interval $[-L, L]$ into N subintervals bounded by grid points at x_j, where $j = 0,\ 1,\ 2,\ 3,\ \ldots,\ N$. These subintervals are not of equal length; rather, the subintervals shorten as we approach the endpoints at $x = -L$ and $x = L$. To determine the positions of the grid points, we construct a semicircle of radius L centered at the origin $x = 0$ and divide the circle into equal sectors. We then project onto the x axis. Thus, the grid points are located at $x_j = L\cos(\pi j/N)$. For all computations done in this paper we take $N = 2^{14} - 1$. The first and last grid points lie at $x = \pm L$, but since N is odd there is no grid point at the origin. We make this choice because the potential $V_4(x)$ is discontinuous at $x = 0$. To find the eigenvalues we impose homogeneous boundary conditions at the endpoints $\pm L$ and finally let L tend to infinity. In all cases we take $L = 10$, 100, and 1000, and we find that the eigenvalues converge rapidly to their $L = \infty$ values.

This paper is organized very simply. In Secs. 2-6 we describe in turn the spectra of $V_n(x)$ for $n = 1$, 2, 3, 4, and 5, and then in Sec. 7 we give some concluding remarks.

2. Eigenvalues for the Scarf-II potential $V_1(x)$

For the potential $V_1(x)$ in (1) we have chosen $A_1 = 30$. In Fig. 1 we plot the eigenvalues in the complex plane for $L = 10$ in panel (a) and for $L = 100$ in panel (b). We observe two kinds of eigenvalues, bound-state eigenvalues, which are indicated by circles, and continuum eigenvalues, which are indicated by crosses in (a) and by dots in (b). As we will see in Fig. 4, we can distinguish between bound-state and continuum eigenvalues by examining the corresponding eigenfunctions. This plot of the absolute values of the eigenfunctions as functions of x shows that the eigenfunctions for bound-state eigenvalues decay smoothly and exponentially to 0 as x approaches the boundaries at $\pm L$ while the continuum eigenfunctions abruptly drop to 0 at one or both boundaries. Note that as L increases from 10 in (a) to 100 in (b), the positions of the bound-state eigenvalues stabilize rapidly but the continuum eigenvalues approach the real axis.

We observe two kinds continuum eigenvalues in Fig. 1. Above a critical value near 28 the continuum eigenvalues are real, but below this critical value the continuum eigenvalues come in complex-conjugate pairs that lie slightly above and below the real axis. These pairs of eigenvalues approach the real axis as L increases but the position of the critical value near $x = 28$ does not change. With increasing L each member of the complex-conjugate pair of eigenvalues approaches the real axis vertically, but as they reach the real axis, one member of the pair moves slightly rightward and the other moves slightly leftward along the real axis, thus doubling the density of points. (This behavior of the continuum eigenvalues is in exact analogy to the motion of the roots

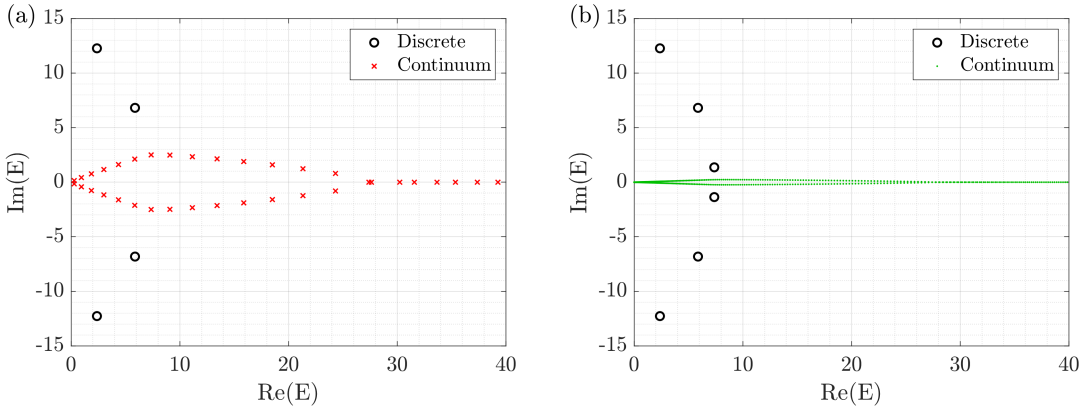


Figure 1. [Color online] Eigenvalues in the complex plane for $V_1(x)$ in (1) with the strength parameter $A_1 = 30$ for the case $L = 10$ in panel (a) and for $L = 100$ in panel (b). Continuum eigenvalues are indicated by red crosses in panel (a) and by green dots in panel (b). Discrete bound-state eigenvalues are indicated by black circles. Note that as L increases, the locations of the bound states stabilize but the continuum eigenvalues all collapse onto the real axis. As they do so, a new complex-conjugate pair of bound states is uncovered. Observe that the continuum eigenvalues come in complex-conjugate pairs until the real parts of these eigenvalues exceeds about 28. Above this critical value the continuum eigenvalues are all real.

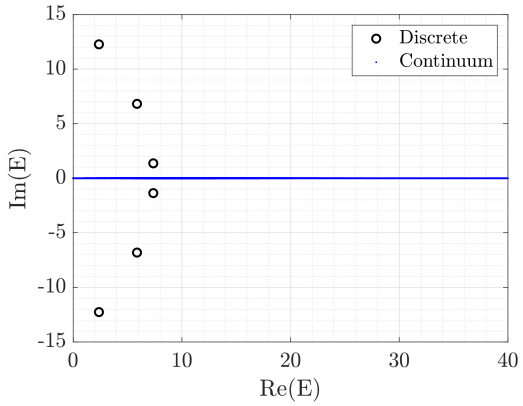


Figure 2. [Color online] Eigenvalues in the complex plane for $V_1(x)$ in (1) with the strength parameter $A_1 = 30$ for the case $L = 1000$. The discrete bound-state eigenvalues (black circles) have not moved but the continuum eigenvalues (blue dots) are now very close to the real axis.

of the famous Wilkenson polynomial [14].) For $L = 1000$, the continuum eigenvalues below $x = 28$ are extremely close to the real axis, but the positions of the complex bound states do not move, as we can see in Fig. 2.

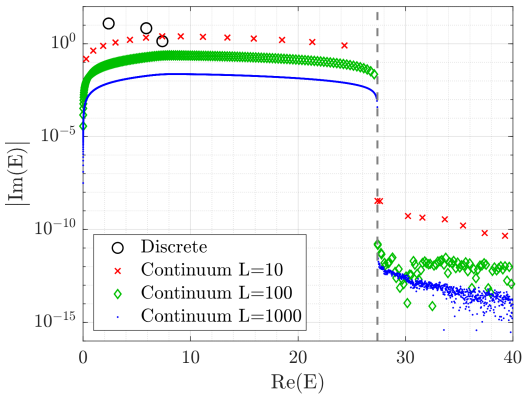


Figure 3. [Color online] Logarithmic plot of the eigenvalue data in Figs. 1 and 2. This plot presents dramatic evidence that the transition from slightly complex continuum eigenvalues to exactly real continuum eigenvalues near $x = 28$ is sharp. There is a jump at the dashed line of about *ten orders of magnitude* at this transition point. Observe that the location of the transition does not change as L is increased from 10 to 100 to 1000.

Figure 3 is a logarithmic plot of the eigenvalues shown in Figs. 1 and 2. Observe that the critical point at $x = 28$ at which the continuum eigenvalues jump from being complex-conjugate pairs to real numbers does not move as L is increased.

To distinguish between discrete and continuum eigenvalues we investigate the behavior of the associated eigenfunctions. Six possible behaviors of the eigenfunctions

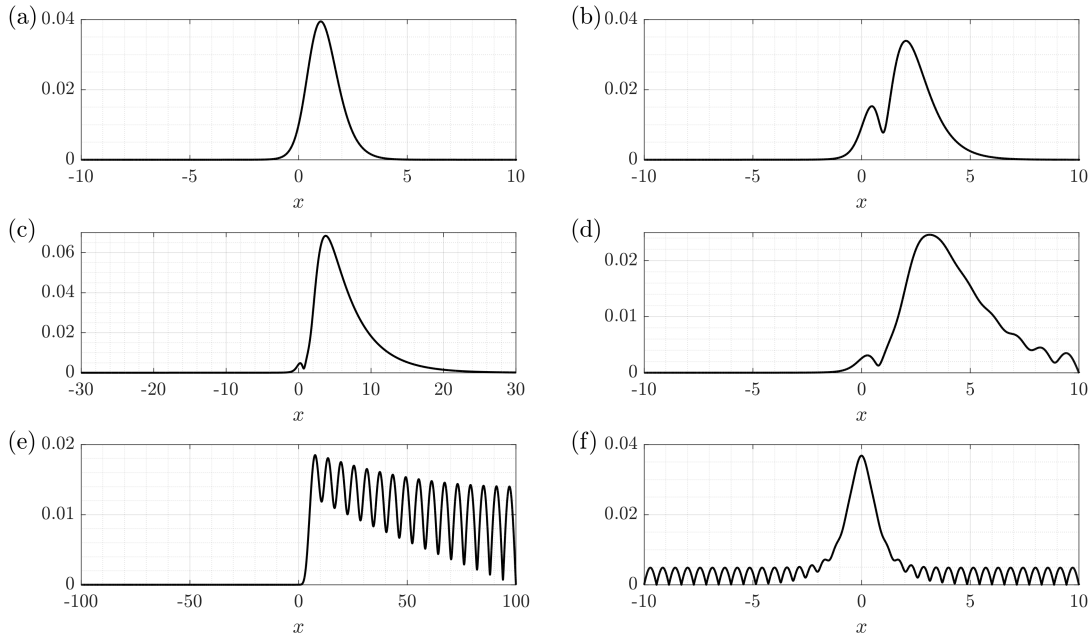


Figure 4. [Color online] Plots of the absolute value of the eigenfunctions associated with some eigenvalues in Fig. 1. Panels (a), (b), and (c) display the eigenfunctions of the three discrete bound-state eigenvalues in panel (b) in Fig. 1: Panel (a) shows the eigenfunction for the eigenvalue $2.374999999702702 + 12.272301129148877\,i$ for $L = 10$; panel (b) shows the eigenfunction for the eigenvalue $5.875000000021835 + 6.817945071620461\,i$ for $L = 10$; panel (c) shows the eigenfunction for the eigenvalue $7.374999997301000 + 1.363589013462076\,i$ for $L = 100$. The next three plots show the behavior of the eigenfunctions for some continuum eigenvalues: Panel (d) shows the eigenfunction for the continuum eigenvalue $7.361943725638523 + 2.501634415578858\,i$ for $L = 10$; panel (e) shows the eigenfunction for the continuum eigenvalue $0.277713365597523 + 0.009073644654185\,i$ for $L = 100$; panel (f) shows the eigenfunction for the continuum eigenvalue $30.234638465149410 + 0.000000000526705\,i$ for $L = 10$. Bound-state eigenfunctions decay smoothly and exponentially as x approaches the endpoints but the continuum eigenfunctions abruptly and sharply drop to 0 at one or both endpoints.

are displayed in Fig. 4. In general, the eigenfunctions of discrete eigenvalues decay smoothly to 0 at the endpoints of the interval but the eigenfunctions of continuum eigenvalues abruptly drop to 0 at one or both endpoints.

3. Eigenvalue behavior of $V_2(x)$

While the potential $V_1(x)$ decays exponentially for large $|x|$, the potential $V_2(x)$ decays algebraically like $|x|^{-3}$ for large $|x|$. Nevertheless, the spectral properties of $V_2(x)$ are strikingly similar to those of $V_1(x)$. For $V_2(x)$ the analog of Fig. 1 is Fig. 5. Again, we have taken the strength parameter A_2 to be 30 and we observe one complex-conjugate pair of bound-state eigenvalues for $L = 10$ in panel (a) and two complex-conjugate pairs of bound-state eigenvalues for $L = 100$ in panel (b). The new pair of bound-state

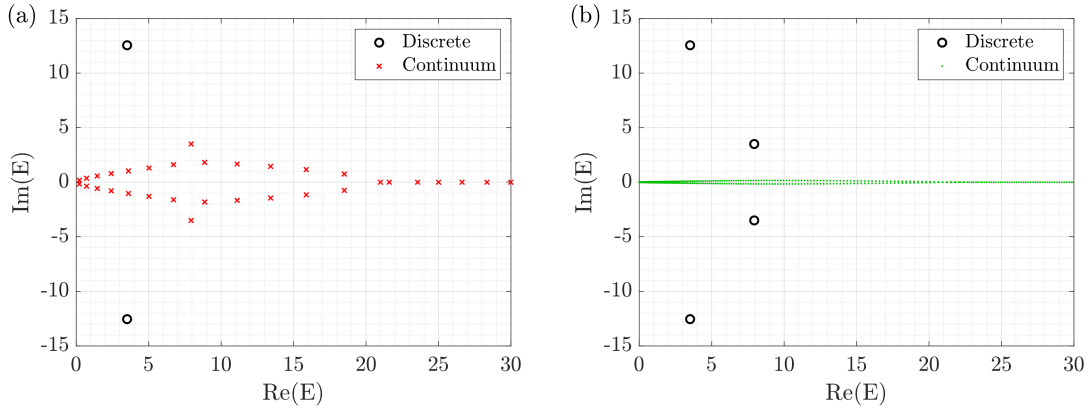


Figure 5. [Color online] Energy spectra for $V_2(x)$ with $A_2 = 30$. Panel (a) shows the eigenvalues for $L = 10$ and panel (b) shows the eigenvalues for $L = 100$. Like the case for the Scarf-II potential $V_1(x)$, the continuum part of the spectrum is slightly complex until the critical point near 21, after which the continuum eigenvalues are real. One pair of bound-state eigenvalues (black circles) is visible in panel (a) but as L is increased to 100 in panel (b), a new pair of bound-state eigenvalues is uncovered.

eigenvalues is uncovered as the continuum eigenvalues collapse towards the real axis.

If we increase L to 1000, we observe in Fig. 6 that the bound-state eigenvalues do not move. However, the continuum eigenvalues lie very close to the real axis.

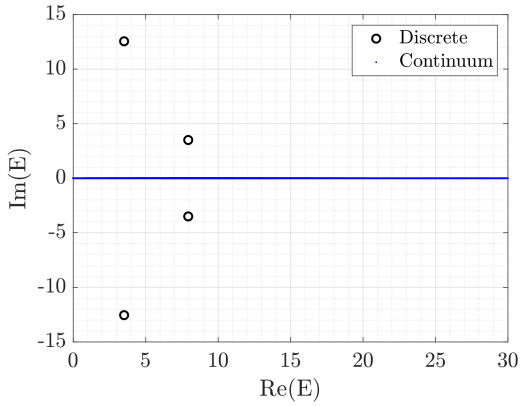


Figure 6. [Color online] Energy eigenvalues for the $V_2(x)$ potential for $A_2 = 30$. For this calculation $L = 1000$. Note that the discrete bound-state energies have not changed from their values in Fig. 5(b). However, the continuum part of the spectrum has moved closer to the real axis.

As with the Scarf-II potential $V_1(x)$, there is a transition in the continuum part of the spectrum that for this model occurs near 21. To examine this transition, we plot the eigenvalues on a logarithmic scale in Fig. 7. Observe that near 21 the continuum eigenvalues undergo an abrupt jump in their imaginary parts of 10 orders of magnitude.

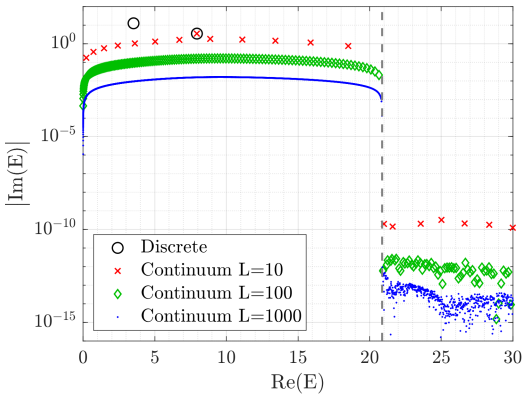


Figure 7. [Color online] Logarithmic plot of the energy eigenvalues for the potential $V_2(x)$ plotted for $L = 10$, 100, and 1000. Like the eigenvalues in Fig. 3, the continuum eigenvalues here undergo an abrupt jump at the dashed line near the critical value close to 21, where the imaginary parts of the continuum eigenvalues suddenly drop by about 10 orders of magnitude. The location of this line is insensitive to the value of L.

4. Eigenvalue behavior of $V_3(x)$

The spectral structure associated with the potential $V_3(x)$ is qualitatively similar to that of $V_2(x)$. We take the strength parameter $A_3 = 30$ and plot the eigenvalues for $L = 10$ in Fig. 8, panel (a), and for $L = 100$ in Fig. 8, panel (b).

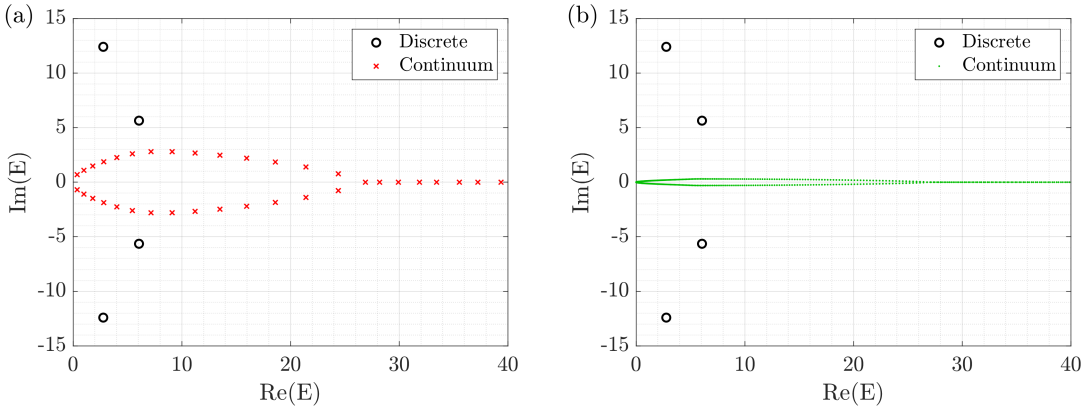


Figure 8. [Color online] Energy eigenvalues for $V_3(x)$ with $A_3 = 30$. In panel (a) we display the data for $L = 10$ and in panel (b) we display the data for $L = 100$. Observe that as L increases, the continuous eigenvalues approach the real axis. However the discrete complex-conjugate bound-state eigenvalues (black circles) remain fixed.

Observe that as L is increased from 10 to 100, the discrete bound-state eigenvalues do not move but the continuum part of the spectrum rapidly approaches the real axis. In Fig. 9 we increase the value of L to 1000. This higher-accuracy calculation shows that the continuum eigenvalues are extremely close to the real axis. However, there is

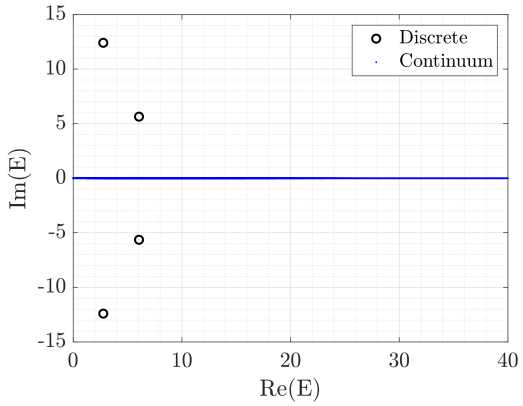


Figure 9. [Color online] Energy eigenvalues for $V_3(x)$ with $A_3 = 30$ calculated at $L = 1000$.

still a critical point where the continuum eigenvalues go from having a small imaginary part to a vanishing imaginary part. This transition point is near 27 and the transition is indicated in Fig. 10 by a dashed line. Once again, the logarithmic plot shows that at the transition the imaginary parts of the continuum eigenvalues abruptly drop by about ten orders of magnitude.

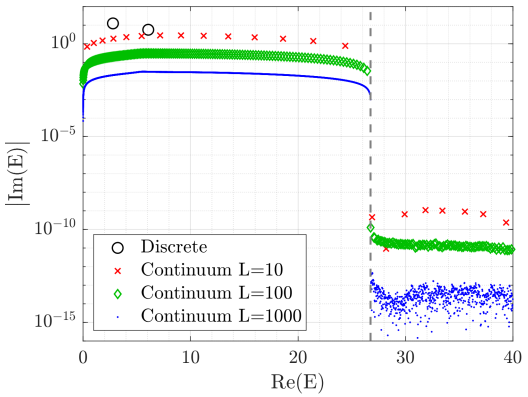


Figure 10. [Color online] Logarithmic plot of the data in Figs. 8 and 9. As in Figs. 3 and 7 we see once again that there is a transition point, in this case near 27, at which the imaginary parts of the continuum eigenvalues suddenly drop by about ten orders of magnitude. The location of this transition, which is indicated by a dashed line, appears to be independent of the choice of L.

5. Eigenvalue behavior of $V_4(x)$

The pattern of eigenvalues associated with $V_4(x)$ is similar to that of $V_1(x)$, $V_2(x)$, and $V_3(x)$. For this potential we take the strength parameter $A_4 = 3$ and plot the spectra

for $L = 10$ and $L = 100$ in Fig. 11 and for $L = 1000$ in Fig. 12. These figures show no qualitatively new features.

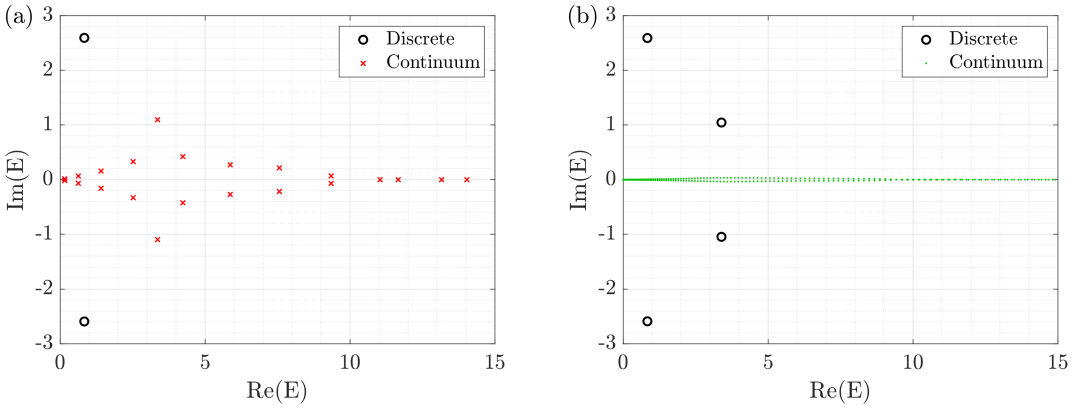


Figure 11. [Color online] Energy eigenvalues associated with $V_4(x)$ for $L = 10$ in panel (a) and for $L = 100$ in panel (b). The strength parameter $A_4 = 3$. One pair of bound-state energies (black circles) can be seen in panel (a) but a new pair becomes visible in Panel (b).

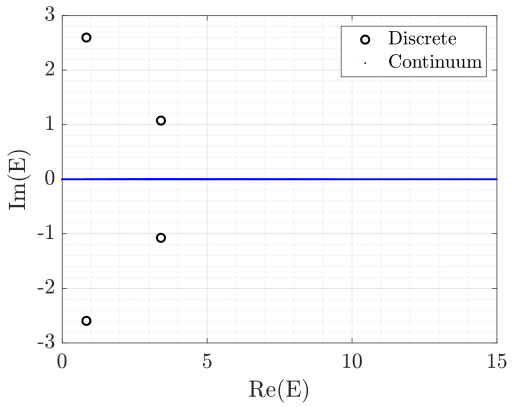


Figure 12. [Color online] Energy eigenvalues for $V_4(x)$ with $A_4 = 3$ for $L = 1000$. Note that the bound-state eigenvalues have not changed from their position from those in panel (b) of Fig. 11.

A logarithmic plot of the eigenvalue data in Figs. 11 and 12 is shown in Fig. 13. Once again we see a transition, in this case near 9.5, at which the continuum eigenvalues abruptly drop in magnitude by about ten orders of magnitude. The location of the transition is again insensitive to the value of L.

6. Eigenvalue behavior of $V_5(x)$

The most interesting and surprising results that we have obtained concern the eigenspectrum associated with $V_5(x)$. For this potential we take the strength parameter

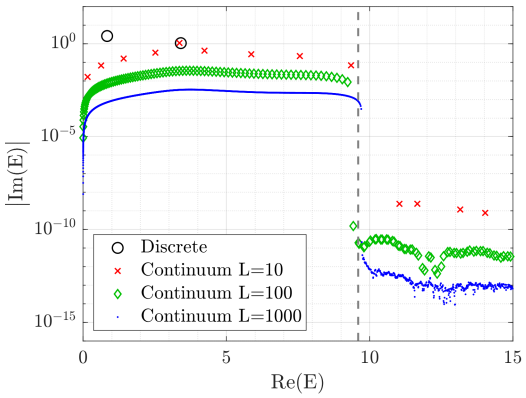


Figure 13. [Color online] Logarithmic plot of the eigenvalue data in Figs. 11 and 12. The data in this figure, like the data in Figs. 3, 7, and 10, indicates that the sharp transition, which in this case is close to 9.5 is not sensitive to the value of L.

$A_5 = 10$. Because this is a long-range potential, it is not easy to obtain accurate and trustworthy numerical results, and we have had to do the $L = 1000$ calculation in *quadruple* precision (for all other results in this paper double precision is sufficient). In Fig. 14 we plot the eigenvalues for $L = 10$ in panel (a) and $L = 100$ in panel (b). There is one pair of bound-state eigenvalues in panel (a). When we increase the size of the interval, we see in panel (b) that the continuum spectrum has dropped much closer to the real axis and has uncovered three new pairs of bound-state eigenvalues.

Figure 14 reveals two new effects that we have not observed in our studies of short-range potentials. First, the sequence of bound-state eigenvalues has *turned around* and is heading backward towards the origin. In Figs. 1, 5, 8, and 11 the real parts of the eigenvalues are increasing, not decreasing. Second, the transition in the continuum part of the spectrum at which the eigenvalues become real is no longer a fixed point on the real axis; rather, the transition point is moving up the real axis as L increases. In panel (a) the transition is near 16 but in panel (b) it is near 28.

If we increase L to 1000, Fig. 15 shows that there are now *nine* complex-conjugate pairs of bound-state eigenvalues (which are not easy to see clearly). This sequence of bound-state eigenvalues is tending towards the origin. To observe the bound-state eigenvalues more clearly we have replotted in Fig. 16 the data in Fig. 15 on a log-log plot. We can see on this plot that the sequence of bound-state eigenvalues is becoming linear.

To observe the transition points in the continuum part of the eigenspectrum, we have plotted the data in Figs. 14 and 15 on a logarithmic graph in Fig. 17. Note that the transition point in the continuum eigenvalues from complex to real is moving up the real axis; it is no longer fixed as it was for finite-range potentials. Observe that at the transition near 40 there is a drop of nearly 20 (and not 10) orders of magnitude. To see this effect requires that we use quadruple and not double precision in our numerical calculations.

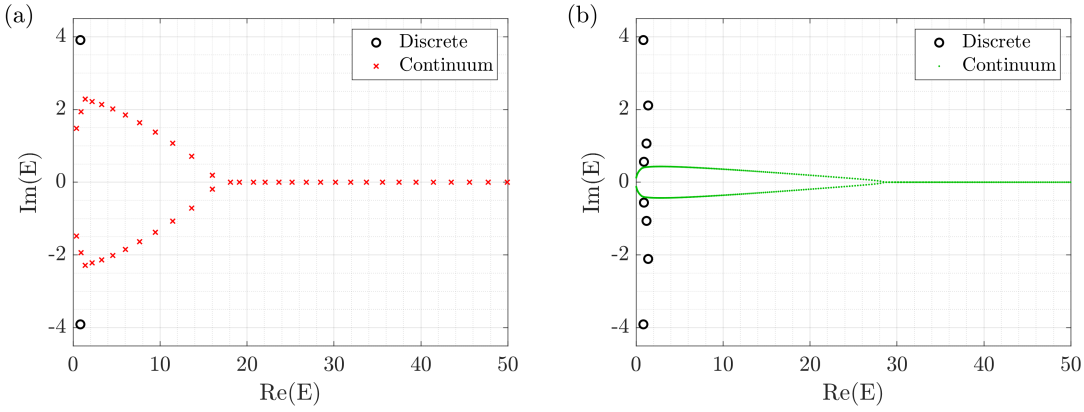


Figure 14. [Color online] Energy eigenvalues associated with $V_5(x)$ with strength parameter $A_5 = 10$. In panel (a) we take $L = 10$ and we observe one complex-conjugate pair of bound-state eigenvalues; in panel (b) we take $L = 100$ and observe three new pairs of complex bound-state eigenvalues. Unlike the results for short-range potentials, this figure shows that the sequence of bound-state eigenvalues is turning around and heading back towards the origin. Also, the transition points in the continuum part of the spectrum are not fixed but are moving up the real axis from about 16 in panel (a) to about 28 in panel (b).

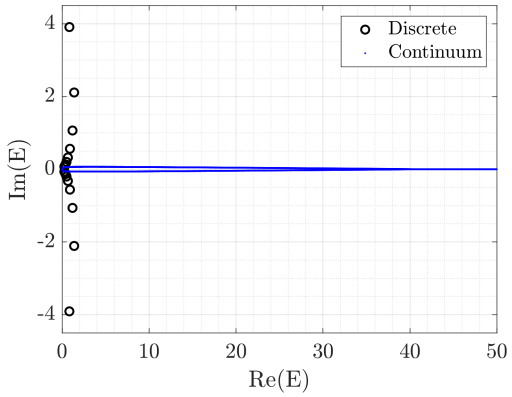


Figure 15. [Color online] Energy eigenvalues associated with $V_5(x)$ with strength parameter $A_5 = 10$. In this figure we have have increased L from 100 in Fig. 14 (right panel) to 1000 and there are now nine complex pairs of bound-state energies (not easy to distinguish). The numerical calculations needed to produce this figure required quadruple precision.

The most interesting aspect of the long-range potential $V_5(x)$ is that it appears to confine an infinite number of bound states and the complex bound-state energies appear to be approaching 0. To verify this we use Richardson extrapolation [14] to study the behavior of the sequence of bound-state energies.

Richardson extrapolation enables one to find the limit of the sequence $\{a_k\}$ as $k \to \infty$ if the limit is a finite number. Given such a sequence we can calculate more

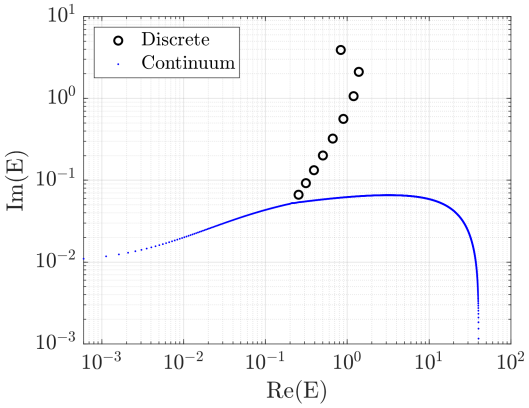


Figure 16. [Color online] Plot of the eigenvalue data in Fig. 15 on a log-log graph. In this plot we can now easily see nine bound-state eigenvalues.

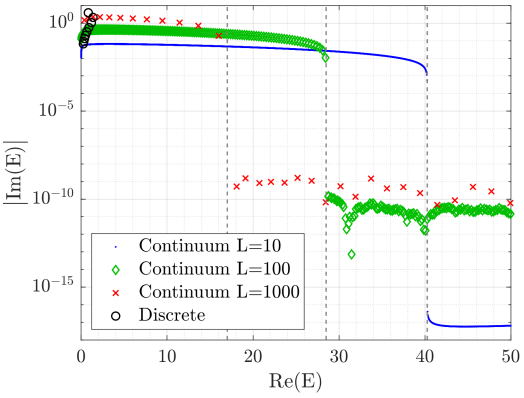


Figure 17. [Color online] Logarithmic plot of the eigenvalue data in Figs. 14 and 15. Observe that the transition point in the continuum part of the spectrum is moving up the real axis as L increases from $L = 10$ to $L = 100$ to $L = 1000$.

and more accurate Richardson extrapolants, which converge faster to the limiting value. The formulas for the first five Richardson extrapolants are given by

$$\begin{aligned}
R_k^{(1)} &= (k+1)a_{k+1} - ka_k, \\
R_k^{(2)} &= \left[(k+2)^2 a_{k+2} - 2(k+1)^2 a_{k+1} + k^2 a_k\right]/2!, \\
R_k^{(3)} &= \left[(k+3)^3 a_{k+3} - 3(k+2)^3 a_{k+2} + 3(k+1)^3 a_{k+1} - k^3 a_k\right]/3!, \\
R_k^{(4)} &= \left[(k+4)^4 a_{k+4} - 4(k+3)^4 a_{k+3} + 6(k+2)^4 a_{k+2}\right. \\
&\qquad \left. -4(k+1)^4 a_{k+1} + k^4 a_k\right]/4!, \\
R_k^{(5)} &= \left[(k+5)^5 a_{k+5} - 5(k+4)^5 a_{k+4} + 10(k+3)^5 a_{k+3}\right. \\
&\qquad \left. -10(k+2)^5 a_{k+2} + 5(k+1)^5 a_{k+1} + k^5 a_k\right]/5!. \qquad (2)
\end{aligned}$$

From our numerical analysis, we have determined that the kth bound-state energy

E_k has the asymptotic form

$$E_k \sim \frac{\alpha}{k^2} \pm i\frac{\beta}{k^3} \qquad (k \gg 1), \tag{3}$$

where α and β are real numbers. This shows that the bound-state eigenvalues associated with $V_5(x)$ share many of the quantitative features of the Balmer series for the hydrogen atom. As indicated in the tables 1 and 2, we have determined that the numerical value of α is about 25 and the numerical value of β is about 61. To obtain these results we have multiplied the real part of E_k by k^2 and the imaginary part of E_k by k^3 and computed the first five Richardson extrapolations.

k	$\mathrm{Re}\, E_k$	$k^2\, \mathrm{Re}\, E_k$	$R_k^{(1)}$	$R_k^{(2)}$	$R_k^{(3)}$	$R_k^{(4)}$	$R_k^{(5)}$
1	0.83298288	0.83298	10.2355	26.6628	29.8431	23.8084	24.2927
2	1.38356468	5.53426	21.1871	29.0481	25.0154	24.2120	25.5106
3	1.19465086	10.7519	25.1176	26.6284	24.4798	25.1396	25.2280
4	0.89645517	14.3433	25.7219	25.5541	24.8568	25.1949	25.0599
5	0.66476032	16.6190	25.6660	25.2553	25.0258	25.1199	—
6	0.50352322	18.1268	25.5486	25.1692	25.0676	—	—
7	0.39157331	19.1871	25.4538	25.1354	—	—	—
8	0.31203794	19.9704	25.3830	—	—	—	—
9	0.25397318	20.5718	—	—	—	—	—

Table 1. Real parts of the first nine eigenvalues E_k $(1 \le k \le 9)$ associated with $V_5(x)$ and the first five Richardson extrapolants constructed from the sequence $\{k^2\, \mathrm{Re}\, E_k\}$. Evidently, the real parts of the eigenvalues vanish like αk^{-2}, where α is roughly 25.

k	$\mathrm{Im}\, E_k$	$k^3\, \mathrm{Im}\, E_k$	$R_k^{(1)}$	$R_k^{(2)}$	$R_k^{(3)}$	$R_k^{(4)}$	$R_k^{(5)}$
1	3.90859038	3.90859	29.8484	63.7004	62.5280	53.5920	61.0166
2	2.10981263	16.8785	52.4164	62.8211	55.3792	59.7791	62.5903
3	1.06386938	28.7245	57.6188	58.3560	58.3125	61.7871	61.3005
4	0.56168819	35.9480	57.9136	58.3342	60.2980	61.4830	60.9267
5	0.32272930	40.3412	58.0538	59.1758	60.8905	61.1739	—
6	0.20043182	43.2933	58.3744	59.8188	61.0165	—	—
7	0.13250064	45.4477	58.7355	60.2180	—	—	—
8	0.09200917	47.1087	59.0650	—	—	—	—
9	0.06644330	48.4372	—	—	—	—	—

Table 2. Imaginary parts of the first nine eigenvalues E_k $(1 \le k \le 9)$ associated with $V_5(x)$ and the first five Richardson extrapolants constructed from the sequence $\{k^3\, \mathrm{Im}\, E_k\}$. The imaginary parts of the eigenvalues vanish like βk^{-3}, where β is roughly 61.

7. Conclusions

In this paper we have studied numerically the five $\mathcal{PT}$-symmetric potentials in (1) that have continuous spectra. Each of these potentials is pure imaginary and vanishes as $|x| \to \infty$. The interesting feature of these potentials is that even though they vanish at $\pm\infty$, they still confine bound states. Of course, an imaginary potential can confine bound states. For example, the ix^3 potential has an infinite number of bound states [1]. However, this potential becomes *stronger* as $|x| \to \infty$. We emphasize that the five potentials that we have studied here *decay* and become *weaker* as $|x| \to \infty$. Even more remarkable is the fact that the potential $V_5(x)$, which decays very slowly as $|x| = \infty$, binds an *infinite* number of bound states and that the sequence of bound-state energies asymptotically approaches the Balmer series for the hydrogen atom.

CMB thanks the Alexander von Humboldt Foundation for partial financial support.

[1] C. M. Bender and S. Boettcher, Phys. Rev. Lett. **80**, 5243 (1998).
[2] C. M. Bender, S. Boettcher, and P. N. Meisinger, J. Math. Phys. **40**, 2201 (1999).
[3] P. E. Dorey, C. Dunning, and R. Tateo, J. Phys. A: Math. Gen. **34**, 5679 (2001).
[4] P. E. Dorey, C. Dunning, and R. Tateo, J. Phys. A: Math. Theor. **40**, R205 (2007).
[5] C. M. Bender, *PT Symmetry: in Quantum and Classical Physics* (World Scientific, Singapore, 2018).
[6] This potential was considered in Z. Ahmed, Phys. Lett. A **282**, 343 (2001) and in the next three references.
[7] Z. Ahmed, D. Ghosh, J. A. Nathan, and G. Parkar, Phys. Lett. A **379**, 2424 (2015).
[8] J. Yang, Opt. Lett. **42**, 4067 (2017).
[9] G. Lévai, Á. Baran, P. Salamon, and T. Verste, Phys. Lett. A **381**, 1936 (2017).
[10] This potential was considered in V. V. Konotop and D. A. Zezyulin, Opt. Lett. **42**, 5206 (2017).
[11] D. N. Christodoulides and J. Yang, eds. 2018 *Parity-time symmetry and its applications* (Springer Tracts in Modern Physics **280**).
[12] C. M. Bender, N. Hassanpour, D. W. Hook, S. P. Klevansky, C. Sunderhauf, and Z. Wen, Phys. Rev. A **95**, 052113 (2017).
[13] L. N. Trefethen, *Spectral Methods in Mattlab* (Society for Industrial and Applied Mathematics, Philadelphia, 2000).
[14] C. M. Bender and S. A. Orszag, *Advanced Mathematical Methods for Scientists and Engineers* (McGraw-Hill, New York, 1978), Chap. 7.